

# Electron-nuclear spin dynamics of $\text{Ga}^{2+}$ paramagnetic centers probed by spin dependent recombination: A master equation approach

V. G. Ibarra-Sierra<sup>1</sup>, J. C. Sandoval-Santana<sup>1</sup>, S. Azaizia<sup>2</sup>, H. Carrère<sup>2</sup>, L.A. Bakaleinikov<sup>3</sup>,  
V. K. Kalevich<sup>3</sup>, E. L. Ivchenko<sup>3</sup>, X. Marie<sup>2</sup>, T. Amand<sup>2</sup>, A. Balocchi<sup>2</sup>, and A. Kunold<sup>4</sup>

<sup>1</sup>*Departamento de Física, Universidad Autónoma Metropolitana Iztapalapa,  
Av. San Rafael Atlixco 186, Col. Vicentina, 09340 Ciudad de México, México*

<sup>2</sup>*Université de Toulouse, INSA-CNRS-UPS, LPCNO,  
135 avenue de Rangueil, 31077 Toulouse, France*

<sup>3</sup>*Ioffe Physical-Technical Institute, 194021 St. Petersburg, Russia*

<sup>4</sup>*Área de Física Teórica y Materia Condensada, Universidad Autónoma Metropolitana Azcapotzalco,  
Av. San Pablo 180, Col. Reynosa-Tamaulipas, 02200 Ciudad de México, México*

(Dated: March 2, 2022)

Similar to nitrogen-vacancy centers in diamond and impurity atoms in silicon, interstitial gallium deep paramagnetic centers in GaAsN have been proven to have useful characteristics for the development of spintronic devices. Among other interesting properties, under circularly polarized light, gallium centers act as spin filters that dynamically polarize free and bound electrons reaching record spin polarizations (close to 100%). Furthermore, the recent observation of the amplification of the spin filtering effect under a Faraday configuration magnetic field has suggested that the hyperfine interaction that couples bound electrons and nuclei permits the optical manipulation of its nuclear spin polarization. Even though the mechanisms behind the nuclear spin polarization in gallium centers are fairly well understood, the origin of nuclear spin relaxation and the formation of an Overhauser-like magnetic field remain elusive. In this work we develop a model based on the master equation approach to describe the evolution of electronic and nuclear spin polarizations of gallium centers interacting with free electrons and holes. Our results are in good agreement with existing experimental observations. In particular, we are able to reproduce the amplification of the spin filtering effect under a circularly polarized excitation in a Faraday configuration magnetic field. In regard to the nuclear spin relaxation, the roles of nuclear dipolar and quadrupolar interactions are discussed. Our findings show that, besides the hyperfine interaction, the spin relaxation mechanisms are key to understand the amplification of the spin filtering effect and the appearance of the Overhauser-like magnetic field. To gain a deeper insight in the interplay of the hyperfine interaction and the relaxation mechanisms, we have also performed calculations in the pulsed excitation regime. Based on our model's results we propose an experimental protocol based on time resolved spectroscopy. It consists of a pump-probe photoluminescence scheme that would allow the detection and the tracing of the electron-nucleus flip-flops through time resolved PL measurements.

## I. INTRODUCTION

Negatively charged nitrogen-vacancy centers in diamond<sup>1–5</sup>, phosphorous atom impurities in silicon<sup>6–11</sup> and other schemes based on point defects embedded in semiconductors have been widely studied as alternatives to develop quantum bits<sup>12,13</sup>. One of the necessary conditions for quantum computing is long electron spin decoherence times to insure a minimum of fault-tolerance<sup>10,14</sup>. In diamond's nitrogen-vacancy centers<sup>15</sup>, silicon vacancies in silicon carbide<sup>16</sup>, silicon<sup>17</sup> and any III-V based quantum dots<sup>10,18</sup> the fluctuating nuclear bath is the main source limiting spin coherence time. The nuclear dipole-dipole interaction is believed to be the dominant mechanism behind the diffusion-induced electron-spin decoherence<sup>19</sup>. To protect the dynamics of the nuclear spins of point defects from the decoherence induced by the environment, semiconductors mainly composed of spin-zero isotopes as silicon and carbon are preferred over III-V semiconductors<sup>5</sup>. Even though the two stable isotopes of Ga, <sup>69</sup>Ga and <sup>71</sup>Ga, have nuclear spin 3/2, in dilute nitride GaAsN, point interstitial defects give rise to paramagnetic centers that have very

peculiar and useful properties. One of them is the spin dependent recombination (SDR)<sup>20–27</sup>. In Ga(In)NAs alloys,  $\text{Ga}_i^{+2}$  paramagnetic centers with only one bound electron can selectively capture another conduction band (CB) electron with the opposite spin orientation<sup>26–30</sup>. Due to this mechanism, paramagnetic centers act as a spin filter that blocks the recombination of CB electrons with the same spin and efficiently capture electrons whose spin is in the opposite direction. In the centers, the bound and captured electron form a singlet state that is destroyed as either one of the electrons recombines to the valence band (VB). It is important to note that while the lifetime of a CB electron with the opposite spin to the paramagnetic electrons is a few pico-seconds, the lifetime of a spin polarized CB electron when the majority of bound electrons are polarized parallel to it may extend to nanoseconds. As a consequence CB electrons spin polarization can reach over 80% under circularly polarized incident light. Additionally the photoluminescence (PL) intensities can be as high as 800% under circularly polarized optical excitation compared to a linearly polarized one<sup>21,22</sup>. The increase in CB electron population allows even for

the detection of electron spin polarization by electrical means due to a giant photoconductivity effect under circularly polarized light<sup>24,31</sup>.

Whereas in diamond and silicon the optical excitation acts directly on the point defects, in GaAsN the bound electron is dynamically spin polarized due to the recombination of spin polarized CB electrons on the paramagnetic centers. Although this mechanism is radically different,  $\text{Ga}_i^{2+}$  centers themselves are very similar to nitrogen vacancies and silicon phosphorous atoms. Recent experiments on GaAsN subject to a weak magnetic field in Faraday configuration<sup>32–35</sup> have shown consistently an enhancement in the spin-filtering mechanism in comparison to the zero magnetic field case. The general agreement among different models<sup>28,35–37</sup> is that the hyperfine interaction (HFI) between the bound electron and the nucleus in the centers is the key element behind this phenomenon. At low magnetic fields, the spin-filtering effect is reduced due to spin state mixing induced by the HFI. For higher values of the magnetic field such that the Zeeman energy exceeds the HFI, the pure bound electron spin states and, consequently, the spin filtering effect are recovered. Even though the role of the HFI is well established, some aspects of these phenomena lacks full understanding. Some observations point to the existence of an Overhauser-like effective magnetic field<sup>32,33</sup> whose origin is yet unclear. It manifests as a shift in the band to band PL intensity or the degree of CB electron spin polarization as functions of the magnetic field. Both features shift to the positive and negative regions of the magnetic field for right and left circularly polarized light respectively. Another aspect that needs further study is the nuclear interaction between  $\text{Ga}_i^{2+}$  centers and adjacent Ga atoms that would lead to nuclear spin relaxation (NSR). The Overhauser-like magnetic field has been correctly reproduced in Ref. [36], however, nuclear spins in this model are assumed to relax very rapidly and the origin of the relaxation mechanism is unclear. On the other hand, the model presented in Ref. [37] considers two phenomenological and arbitrary NSR times for traps with one and two bound electrons. Despite the improvements in this work, the model considers Ga centers with 1/2 nuclear spins instead of 3/2 in order to simplify the kinetic equations.

In this paper we examine the spin dynamics in GaAsN alloys. We propose a model based on the master equation for the density matrix that describes the main interactions between CB electrons, VB holes and paramagnetic traps. It addresses the problems on spin relaxation mechanisms and Overhauser-like magnetic field. In fact, our results show that the Overhauser-like magnetic field strongly depends on the NSR times and the mechanisms behind them.

The model developed here is based on the preexisting two charge model (TCM)<sup>20,21,27,29</sup>. In addition to the SDR processes, it contains the mechanisms that give rise so NSR and HFI. NSR is addressed through the Wangness, Bloch, and Redfield relaxation theory<sup>38–41</sup>.

Two interactions are explored as possible candidates to produce the NSR: dipolar interaction between neighbouring nuclei<sup>38</sup> and quadrupolar<sup>38,42</sup> interaction with charge fluctuations in the environment.

To further explore the role of HFI in Ga centers, we have studied the time resolved electronic and nuclear spin polarizations under pulsed excitation. Using these results we outline a method based on a pump-probe photoluminescence scheme to trace the coherent evolution of coupled electrons and nuclear spins as they flip-flop due to the HFI.

This paper is organized as follows. In Sec. II we introduce the master equation model that describes the key processes in the spin dynamics of electrons and nuclei in GaAsN. The role of the HFI and the NSR mechanism are discussed in this section. The mathematical forms of the dipolar and quadrupolar dissipators are introduced in Sec. IID. In Sec. III A we establish the main mechanism behind the nuclear spin relaxation in  $\text{Ga}_i^{2+}$  centers by comparing the theoretical results issued by the model with previously existing experimental results. Simulations in the pulsed excitation regime are presented in Sec. IIIB. In Sec. IV we summarize the main results.

## II. MASTER EQUATION

The system mainly consists of four elements: VB holes, CB electrons, unpaired traps (UT) and paired traps (PT). Whereas VB holes' spin relaxes with a characteristic times below 1 ps<sup>43</sup>, CB electronic spin relaxes on a typical time in the range 100 – 400 ps<sup>25,44</sup>. Therefore, for the sake of simplicity, we consider VB holes to be unpolarized and electrons may occupy spin-up or spin-down states. Gallium paramagnetic traps or UTs can be understood as a 3/2 nuclear spin coupled to a 1/2 bound electron spin via HFI. On the other hand, when a PT is formed if a CB electron is captured by an UT, the bound and captured electrons form a singlet state that cannot interact with the nuclear spin. Thus the quantum state basis that describes this system must have: (i) one state for holes in the VB, (ii) two states for the spin up and spin down CB electrons, (iii) eight states that account for the nucleus-bound electron system in the UTs and (iv) four states for the nuclear spin in the PTs. The complete quantum state basis is therefore given by

$$\begin{aligned} \mathcal{B} = \left\{ |1\rangle = |h\rangle, |2\rangle = |\downarrow\rangle, |3\rangle = |\uparrow\rangle, |4\rangle = |-\frac{3}{2}, \downarrow\rangle, \right. \\ |5\rangle = |-\frac{1}{2}, \downarrow\rangle, |6\rangle = |\frac{1}{2}, \downarrow\rangle, |7\rangle = |\frac{3}{2}, \downarrow\rangle, \\ |8\rangle = |-\frac{3}{2}, \uparrow\rangle, |9\rangle = |-\frac{1}{2}, \uparrow\rangle, |10\rangle = |\frac{1}{2}, \uparrow\rangle, \\ |11\rangle = |\frac{3}{2}, \uparrow\rangle, |12\rangle = |-\frac{3}{2}, \uparrow\downarrow\rangle, \\ \left. |13\rangle = |-\frac{1}{2}, \uparrow\downarrow\rangle, |14\rangle = |\frac{1}{2}, \uparrow\downarrow\rangle, |15\rangle = |\frac{3}{2}, \uparrow\downarrow\rangle \right\}, \quad (1) \end{aligned}$$

where  $|h\rangle$  is the VB hole state and  $|\uparrow\rangle$  and  $|\downarrow\rangle$  are the spin-up and spin-down CB electron states respectively. The following eight states  $|- \frac{3}{2}, \downarrow\rangle, |-\frac{1}{2}, \downarrow\rangle, \dots, |\frac{3}{2}, \uparrow\rangle$  are the bound-electron and nuclear spin states projected along the  $z$  axis corresponding to the UT. Finally, the PTs are described by the nuclear-spin states  $|- \frac{3}{2}, \uparrow\downarrow\rangle, \dots, |\frac{3}{2}, \uparrow\downarrow\rangle$ .

The dynamics of the four parts of the system and their interactions can be described through the master equation

$$\frac{d\hat{\rho}}{dt} = \frac{i}{\hbar} [\hat{\rho}, \hat{H}] + \mathcal{D}(\hat{\rho}), \quad (2)$$

where  $\hat{\rho}$  is the density matrix,  $\hat{H}$  is the Hamiltonian and  $\mathcal{D}(\hat{\rho})$  is the dissipator. The Hamiltonian contains the internal interactions among the four components of the system. We are interested in the combined effect of an external magnetic field and the HFI in Ga centers, therefore the Hamiltonian must contain Zeeman and HFI terms. The interactions among the different parts of the system and the surroundings are accounted for by the Dissipator. These are mostly interactions with the electromagnetic field, occurring during recombination or excitation processes, or interactions with the nuclear spin environment. The main processes introduced in our model are schematized in Fig. 1.

#### A. Hamiltonian: Zeeman and hyperfine interactions

The Hamiltonian is given by

$$\hat{H} = \hbar\omega \cdot \hat{\mathbf{S}} + \hbar\Omega \cdot \hat{\mathbf{S}}_c + A\hat{\mathbf{I}}_1 \cdot \hat{\mathbf{S}}_c. \quad (3)$$

The first and second terms in the Hamiltonian correspond to the Zeeman interaction for CB and bound electrons in Ga centers respectively. In these terms  $\omega = g\mu_B \mathbf{B}/\hbar$ ,  $\Omega = g_c\mu_B \mathbf{B}/\hbar$ ,  $\mathbf{B}$  is the external magnetic field,  $\mu_B$  is the Bohr magneton and,  $g$  and  $g_c$  are the CB and bound electrons gyromagnetic factors. The HFI term, the third one on the right-hand side of Eq. (3), couples the bound electron and the nuclear spin in UTs. The hyperfine parameter is given by  $A$ .

The spin operator for CB electrons that appears in the first Zeeman term of the Hamiltonian is  $\hat{\mathbf{S}} = (\hat{S}_x, \hat{S}_y, \hat{S}_z)$ . In UTs, the bound electron spin and nuclear spin operators entering the HFI term are  $\hat{\mathbf{S}}_c = (\hat{S}_{cx}, \hat{S}_{cy}, \hat{S}_{cz})$ , and  $\hat{\mathbf{I}}_1 = (\hat{I}_{1x}, \hat{I}_{1y}, \hat{I}_{1z})$  respectively. As the singlet state formed in the PTs interacts neither with the external magnetic field nor with their nuclear spin  $\hat{\mathbf{I}}_2 = (\hat{I}_{2x}, \hat{I}_{2y}, \hat{I}_{2z})$ , it does not appear in the Hamiltonian.

#### B. Density matrix operator space

The relaxation mechanisms of CB electrons and nuclei in the Ga centers are described by the dissipator  $\mathcal{D}(\hat{\rho})$ .

Also, the photoexcitation and recombination of electrons will be accounted for by  $\mathcal{D}$ .

Our approach to formulating a suitable dissipator consists in expanding the relevant operators as linear combination of the elements of an operator vector space. In principle this set should be formed in the basis (1) by linearly independent  $15 \times 15$  Hermitian matrices. However, the density matrix structure is considerably simplified by assuming that the four components of the system (CB, UT, PT, VB) are interconnected only by the dissipator. As the four parts of the system are exclusively coupled by the recombination or excitation processes, this is a reasonable assumption. Thus, the density matrix operator can be presented in the block diagonal form:

$$\hat{\rho} = \begin{pmatrix} \hat{\rho}_{\text{VB}} & & & \\ & \hat{\rho}_{\text{CB}} & & \\ & & \hat{\rho}_1 & \\ & & & \hat{\rho}_2 \end{pmatrix} \quad (4)$$

where the four blocks  $\hat{\rho}_{\text{VB}}$  ( $1 \times 1$ ),  $\hat{\rho}_{\text{CB}}$  ( $2 \times 2$ ),  $\hat{\rho}_1$  ( $8 \times 8$ ) and  $\hat{\rho}_2$  ( $4 \times 4$ ) are the partial density matrices of VB holes, CB electrons, UTs and PTs respectively. Given that  $\hat{\rho}$  takes the form of a block diagonal matrix since no coherences can arise between the four components, it suffices to consider the smaller vector space of 85 Hermitian matrices that generate the four blocks.

We start by finding an internal space of Hermitian matrices

$$\Lambda = \{\hat{\lambda}_1, \hat{\lambda}_2, \dots, \hat{\lambda}_n\}, \quad (5)$$

that spans the  $n = 85$  relevant elements of the  $15 \times 15$  matrix. The generators in this set can be chosen in such a way that they are Hermitian and orthogonal with respect to the scalar product given by the trace

$$\langle \hat{\lambda}_i, \hat{\lambda}_j \rangle \equiv \text{Tr} [\hat{\lambda}_i^\dagger \hat{\lambda}_j] = \delta_{i,j} \text{Tr} [\hat{\lambda}_i^2]. \quad (6)$$

This choice conveniently links the inner product with the expected value of a given operator  $\hat{O}$

$$O = \text{Tr} [\hat{O} \hat{\rho}] = \langle \hat{\rho}, \hat{O} \rangle, \quad (7)$$

acting on  $\hat{\rho}$ . In this manner any operator can be expanded as a linear combination of the elements of (5) as

$$\hat{O} = \sum_{q=1}^{85} \frac{\text{Tr} [\hat{\lambda}_q \hat{O}]}{\text{Tr} [\hat{\lambda}_q^2]} \hat{\lambda}_q. \quad (8)$$

A very convenient set of operators is the one formed by the generators of the unitary groups  $U(1)$  (VB holes),  $U(2)$  (CB electrons),  $U(4)$  (PTs) and  $U(8)$  (UTs). The operators forming this set are not only of physical significance but they are also linearly independent and orthogonal with respect to the trace. Explicitly, the set of operators in (5) is given by

$$\Lambda = \{\hat{\rho}, \hat{S}_i, \hat{U}_{k,j,i}, \hat{T}_{j,i}\}, \quad i, j, k = 0, 1, 2, 3; \quad (9)$$

where  $\hat{p}$ ,  $\hat{S}_i$ ,  $\hat{U}_{k,j,i}$  and  $\hat{T}_{j,i}$  generate the VB, CB, UT and PT blocks. The VB hole population density operator can be represented by the matrix

$$\hat{p} = \begin{pmatrix} 1 & & & \\ & \hat{0}_{2 \times 2} & & \\ & & \hat{0}_{8 \times 8} & \\ & & & \hat{0}_{4 \times 4} \end{pmatrix}. \quad (10)$$

The operators that generate the the CB block can be compiled in the matrix

$$\hat{S}_i = \begin{pmatrix} 0 & & & \\ & \hat{s}_i & & \\ & & \hat{0}_{8 \times 8} & \\ & & & \hat{0}_{4 \times 4} \end{pmatrix}, \quad i = 0, 1, 2, 3, \quad (11)$$

where the electron population density in the CB is given by  $\hat{n} = \hat{S}_0$  and their spin operators are  $\hat{S}_i$  for  $i = 1, 2, 3$ . Here  $\hat{s}_0 = \hat{1}_{2 \times 2}$  is the  $2 \times 2$  identity matrix, and  $\hat{s}_i$  for  $i = 1, 2, 3$  are the standard Pauli spin matrices that fulfill the usual spin commutation relations

$$[\hat{s}_i, \hat{s}_j] = i \sum_{k=1,2,3} \epsilon_{ijk} \hat{s}_k. \quad (12)$$

This definition allows us to write the matrices that generate the UT and PT blocks in the compact forms

$$\hat{U}_{k,j,i} = \begin{pmatrix} 0 & & & \\ & \hat{0}_{2 \times 2} & & \\ & & \hat{s}_k \otimes \hat{s}_j \otimes \hat{s}_i & \\ & & & \hat{0}_{4 \times 4} \end{pmatrix}, \quad (13)$$

and

$$\hat{T}_{j,i} = \begin{pmatrix} 0 & & & \\ & \hat{0}_{2 \times 2} & & \\ & & \hat{0}_{8 \times 8} & \\ & & & \hat{s}_j \otimes \hat{s}_i \end{pmatrix}. \quad (14)$$

According to this scheme the population density of UTs is  $\hat{N}_1 = \hat{U}_{0,0,0}$ , and the one for PTs is  $\hat{N}_2 = \hat{T}_{0,0}$ . Similarly, the CB electrons' spin operators are:  $\hat{S}_x = \hat{S}_1$ ,  $\hat{S}_y = \hat{S}_2$  and  $\hat{S}_z = \hat{S}_3$ . We have the same case for the bound electron spin operator components in UTs where  $\hat{S}_{cx} = \hat{U}_{1,0,0}$ ,  $\hat{S}_{cy} = \hat{U}_{2,0,0}$  and  $\hat{S}_{cz} = \hat{U}_{3,0,0}$ . The operators of the nuclear spin of UTs and PTs can be expressed as linear combinations of the elements of  $\Lambda$  as

$$\hat{I}_1 = \mathcal{M} \hat{\mathcal{U}}, \quad (15)$$

$$\hat{I}_2 = \mathcal{M} \hat{\mathcal{T}}, \quad (16)$$

where

$$\hat{\mathcal{U}}^\top = (\hat{U}_{0,0,1}, \hat{U}_{0,1,1}, \hat{U}_{0,2,2}, \hat{U}_{0,0,2}, \hat{U}_{0,1,2}, \hat{U}_{0,2,1}, \hat{U}_{0,0,3}, \hat{U}_{0,3,0}), \quad (17)$$

$$\hat{\mathcal{T}}^\top = (\hat{T}_{0,1}, \hat{T}_{1,1}, \hat{T}_{2,2}, \hat{T}_{0,2}, \hat{T}_{1,2}, \hat{T}_{2,1}, \hat{T}_{0,3}, \hat{T}_{3,0}), \quad (18)$$

and

$$\mathcal{M} = \begin{bmatrix} \sqrt{3} & 2 & 2 & 0 & 0 & 0 & 0 & 0 \\ 0 & 0 & 0 & \sqrt{3} & -2 & 2 & 0 & 0 \\ 0 & 0 & 0 & 0 & 0 & 0 & 1 & 2 \end{bmatrix}. \quad (19)$$

### C. Dissipator

The dissipator can be separated in six parts

$$\mathcal{D}(\hat{\rho}) = \hat{\mathcal{G}} + \hat{\mathcal{D}}_{\text{SDR}} + \hat{\mathcal{D}}_S + \hat{\mathcal{D}}_{\text{SC}} + \hat{\mathcal{D}}_1 + \hat{\mathcal{D}}_2. \quad (20)$$

Here  $\hat{\mathcal{G}}$  contains the VB hole and CB electron photogeneration terms. The SDR processes that mainly consist of the selective capture of CB electrons in UTs according to their relative spin orientation and the subsequent recombination to the VB are described by the  $\hat{\mathcal{D}}_{\text{SDR}}$  dissipator. CB and bound electron spin relaxation are accounted by  $\hat{\mathcal{D}}_S$  and  $\hat{\mathcal{D}}_{\text{SC}}$ . NSR in UT's and PT's is introduced through the dissipators  $\hat{\mathcal{D}}_1$  and  $\hat{\mathcal{D}}_2$ .

The term  $\hat{\mathcal{G}}$  that models the generation of electrons is given by

$$\hat{\mathcal{G}} = (G_\uparrow + G_\downarrow)(\hat{p} + \hat{n}) + 2(G_\uparrow - G_\downarrow)\hat{e} \cdot \hat{\mathbf{S}}, \quad (21)$$

where  $G_\uparrow$  and  $G_\downarrow$  are the spin up and spin down electron generation rates. The unitary vector  $\hat{e}$  points in the direction of the incident light.

To build the  $\mathcal{D}_{\text{SDR}}$  part of the dissipator we resort to the TCM<sup>20,21,27,29</sup> given by the following kinetic equations ( $\hbar=1$ )

$$\dot{n} = -c_n(nN_1 - 4\mathbf{S} \cdot \mathbf{S}_c) + G_\uparrow + G_\downarrow, \quad (22)$$

$$\dot{p} = -c_p N_2 p + G_\uparrow + G_\downarrow, \quad (23)$$

$$\dot{N}_1 = -c_n(nN_1 - 4\mathbf{S} \cdot \mathbf{S}_c) + c_p N_2 p, \quad (24)$$

$$\dot{N}_2 = c_n(nN_1 - 4\mathbf{S} \cdot \mathbf{S}_c) - c_p N_2 p. \quad (25)$$

$$\begin{aligned} \dot{\mathbf{S}} = & -c_n(\mathbf{S}N_1 - \mathbf{S}_c n) - \frac{1}{\tau_s} \mathbf{S} + \boldsymbol{\omega} \times \mathbf{S} \\ & + \frac{G_\uparrow - G_\downarrow}{2} \hat{e}, \end{aligned} \quad (26)$$

$$\dot{\mathbf{S}}_c = -c_n(\mathbf{S}_c n - \mathbf{S}N_1) - \frac{1}{\tau_{sc}} \mathbf{S}_c + \boldsymbol{\Omega} \times \mathbf{S}_c. \quad (27)$$

In the previous equations, the population densities of CB electrons and VB holes are given by  $n$  and  $p$  respectively. The density of UTs is  $N_1$ ,  $N_2$  is the density of electron singlets hosted by the centers (PTs), and consequently  $N_c = N_1 + N_2$  is the total density of Ga centers. The vectors  $\mathbf{S}$  and  $\mathbf{S}_c$  represent the average of free and bound electron spin polarizations. The spin dependent capture of electrons in the Ga centers is ensured by the recombination rate terms  $c_n(nN_1 - 4\mathbf{S} \cdot \mathbf{S}_c)$  and  $c_n(\mathbf{S}N_1 - \mathbf{S}_c n)$  where  $c_n$  is a constant. Notice that these two terms vanish when the system is fully polarized, i.e.  $S_z = n/2$ ,  $S_x = S_y = 0$ ,  $S_{cz} = N_1/2$  and  $S_{cx} = S_{cy} = 0$ . The recombination rate of one of the electrons trapped in the Ga centers to the VB is given by the terms  $c_p N_2 p$  where  $c_p$  is a constant. We thus require that the dissipator's structure is such that the master equation reduces to Eqs. (22)-(27) when the HFI is lifted ( $A = 0$ ). This may be achieved by identifying  $n$ ,  $p$ ,  $N_1$ ,  $N_2$ ,  $\mathbf{S}$  and  $\mathbf{S}_c$  with the quantum statistical average of the corresponding operators, namely  $n = \text{Tr}[\hat{\rho}\hat{n}]$ ,  $p = \text{Tr}[\hat{\rho}\hat{p}]$ ,  $N_1 = \text{Tr}[\hat{\rho}\hat{N}_1]$ ,

$N_2 = \text{Tr}[\hat{\rho}\hat{N}_2]$ ,  $\mathbf{S} = \text{Tr}[\hat{\rho}\hat{\mathbf{S}}]$  and  $\mathbf{S}_c = \text{Tr}[\hat{\rho}\hat{\mathbf{S}}_c]$ . As well, the quantum statistical average of any generator of  $\Lambda$  is given by  $\lambda_q = \text{Tr}[\hat{\rho}\hat{\lambda}_q]$  and therefore, the density matrix can be expanded as

$$\hat{\rho} = \sum_{q=1}^{85} \frac{\text{Tr}[\hat{\rho}\hat{\lambda}_q]}{\text{Tr}[\hat{\lambda}_q^2]} \hat{\lambda}_q = \sum_{q=1}^{85} \frac{\lambda_q}{\text{Tr}[\hat{\lambda}_q^2]} \hat{\lambda}_q. \quad (28)$$

The SDR part of the dissipator  $\hat{\mathcal{D}}_{\text{SDR}}$  can also be expanded in terms of the elements of  $\Lambda$  as

$$\hat{\mathcal{D}}_{\text{SDR}} = \sum_{q=1}^{85} \frac{C[\hat{\lambda}_q]}{\text{Tr}[\hat{\lambda}_q^2]} \hat{\lambda}_q = \sum_{q=1}^{85} \frac{C_q}{\text{Tr}[\hat{\lambda}_q^2]} \hat{\lambda}_q. \quad (29)$$

To determine the coefficients  $C_q \equiv C[\hat{\lambda}_q] = \text{Tr}[\hat{\lambda}_q \hat{\mathcal{D}}_{\text{SDR}}]$  we insert (29) in the master equation (2) and multiply by  $\hat{n}$ ,  $\hat{p}$ ,  $\hat{N}_1$ ,  $\hat{N}_2$ ,  $\hat{\mathbf{S}}$  or  $\hat{\mathbf{S}}_c$ . By taking the trace of the resulting equation we readily find the coefficients

$$C[\hat{p}] = -c_p p N_2, \quad (30)$$

$$C[\hat{n}] = -c_n (n N_1 - 4 \mathbf{S} \cdot \mathbf{S}_c), \quad (31)$$

$$C[\hat{N}_1] = -c_n (n N_1 - 4 \mathbf{S} \cdot \mathbf{S}_c) + c_p N_2 p, \quad (32)$$

$$C[\hat{N}_2] = c_n (n N_1 - 4 \mathbf{S} \cdot \mathbf{S}_c) - c_p N_2 p, \quad (33)$$

$$C[\hat{\mathbf{S}}] = -c_n (\mathbf{S} N_1 - \mathbf{S}_c n), \quad (34)$$

$$C[\hat{\mathbf{S}}_c] = -c_n (\mathbf{S}_c n - \mathbf{S} N_1). \quad (35)$$

At this point we have considerable freedom since these equations only define 10 of the 85 coefficients needed to fully determine the  $\hat{\mathcal{D}}_{\text{SDR}}$  dissipator. However, the choices get narrowed down by imposing the symmetry and invariance properties that the system is expected to satisfy. As the most basic requirement, the master equation must be invariant under any arbitrary rotation in accordance with the space's isotropy. The tensors  $\hat{T}_{j,i}$  and  $\hat{U}_{k,j,i}$  must therefore transform by the corresponding laws. The complete set of coefficients is thus given by

$$C[\hat{p}] = -c_p p T_{0,0}, \quad (36)$$

$$C[\hat{n}] = -c_n \left( S_0 U_{0,0,0} - 4 \sum_{r=1}^3 S_r U_{r,0,0} \right), \quad (37)$$

$$C[\hat{S}_k] = -c_n (S_k U_{0,0,0} - S_0 U_{k,0,0}), \quad (38)$$

$$C[\hat{U}_{0,j,i}] = c_p p T_{j,i} - c_n \left( S_0 U_{0,j,i} - 4 \sum_{r=1}^3 S_r U_{r,j,i} \right), \quad (39)$$

$$C[\hat{U}_{k,j,i}] = -c_n (S_0 U_{k,j,i} - S_k U_{0,j,i}), \quad (40)$$

$$C[\hat{T}_{j,i}] = -c_p p T_{j,i} + c_n \left( S_0 U_{0,j,i} - 4 \sum_{r=1}^3 S_r U_{r,j,i} \right), \quad (41)$$

where  $i, j = 0, 1, 2, 3$  and  $k = 1, 2, 3$ . The spin precession terms  $\boldsymbol{\omega} \times \mathbf{S}$  and  $\boldsymbol{\Omega} \times \mathbf{S}_c$ , absent in Eqs. (36)-(41), are accounted for by the Zeeman terms in the Hamiltonian (3) since they concern the coherent evolution of the system.

The SDR part of the dissipator also excludes the spin relaxation of CB and bound electrons. These terms enter the dissipator through  $\hat{\mathcal{D}}_S$  and  $\hat{\mathcal{D}}_{\text{SC}}$  as

$$\hat{\mathcal{D}}_S = -\frac{1}{\tau_s} \sum_{q=3}^5 \frac{\lambda_q}{\text{Tr}[\hat{\lambda}_q^2]} \hat{\lambda}_q = -\frac{2}{\tau_s} \sum_{i=1}^3 S_i \hat{S}_i, \quad (42)$$

$$\hat{\mathcal{D}}_{\text{SC}} = -\frac{2}{\tau_{sc}} \sum_{i=1}^3 S_{ci} \hat{S}_{ci}. \quad (43)$$

The CB electron spin relaxation time due to the Dyakonov-Perel mechanism is given by  $\tau_s$ , while  $\tau_{sc}$  is the phenomenological bound electron spin relaxation time in Ga centers<sup>36,37</sup>. The dissipators (42) and (43) yield the CB and bound electron spin relaxation terms  $\mathbf{S}/\tau_s$  and  $\mathbf{S}_c/\tau_{sc}$  in the TCM.

#### D. Nuclear spin relaxation

To get an insight into the role of the possible mechanisms involved in NSR we consider three different models: non-selective, dipolar and quadrupolar. As a reference we also study the effects of the absence of spin relaxation. The dipolar and quadrupolar interactions are dealt through the Wangsness, Bloch, and Redfield relaxation theory<sup>38-41</sup> summarized in Appendix A.

First, we study the non-selective<sup>37</sup> dissipators for UTs and PTs given by

$$\left( \hat{\mathcal{D}}_1 \right)_{sm,s'm'} = -\frac{1}{\tau_{n1}} \left( \rho_{1;s,m;s',m'} - \frac{\delta_{m,m'}}{4} \sum_{m''=-3/2}^{3/2} \rho_{1;s,m'';s',m''} \right); \quad (44)$$

$$\left( \hat{\mathcal{D}}_2 \right)_{m,m'} = -\frac{1}{\tau_{n2}} \left( \rho_{2;m,m'} - \frac{\delta_{m,m'}}{4} \sum_{m''=-3/2}^{3/2} \rho_{2;m'',m''} \right), \quad (45)$$

where  $s = -1/2, 1/2$  and  $m = -3/2, -1/2, 1/2, 3/2$  are the bound electron spin and nuclear spin indices. This dissipator is highly symmetrical.

Second, we consider the relaxation due to the dipolar interactions between neighbouring Ga nuclei. In this case, the Hamiltonian (A1) only contains the irreducible spherical tensors of rank  $k = 1$ . The terms in this Hamiltonian correspond to the angular momentum operators interacting with a random local field. Substituting (A6)

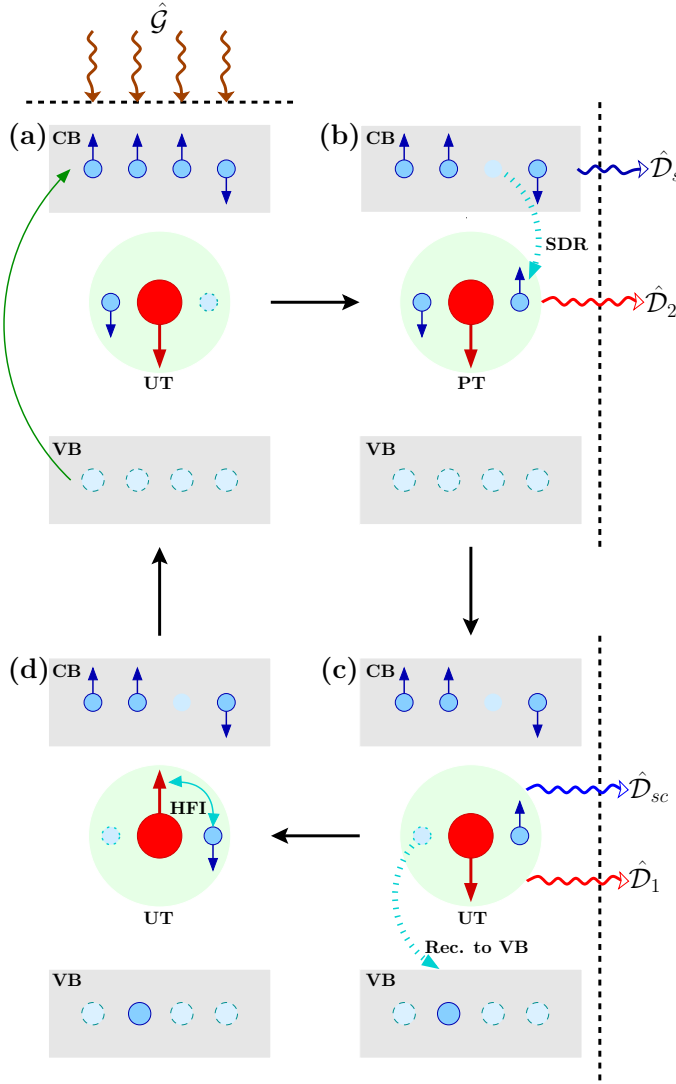


Figure 1. Schematic diagram of the processes involved in the nuclear spin polarization of Ga centers. The flow of the angular momentum is also shown. Following the selection rules of GaAs, three spin up, one spin down CB electrons and 4 unpolarized VB holes are generated by four photons with 100% left circular polarization (a). The angular momentum of photons is transferred to the CB electrons. Traps whose bound electrons are spin polarized in the opposite direction to the majority of the CB electrons' spin, can capture CB electrons with opposite spin orientation forming a spin singlet (b). This process partly transfers angular momentum from the CB electrons to the bound electrons in traps. Simultaneously CB electrons' spin and PT's nuclear spins relax due to  $\mathcal{D}_S$  and  $\mathcal{D}_2$  making the system loose angular momentum to the environment. As one of the trapped electrons recombines to the VB the spin singlet in the PT is dissociated and becomes a UT (c). At the same time, the bound electron and nuclear spins in the UT relax due to the  $\mathcal{D}_{SC}$  and  $\mathcal{D}_1$  dissipators (c). Again the system loses angular momentum to the environment. At this stage the bound electron and the nucleus are able to interact via the HFI and angular momentum is exchanged (in the presented case) between them by a series of flip-flops (d). From (d) to (a) the center can capture a new electron and the cycle starts again.

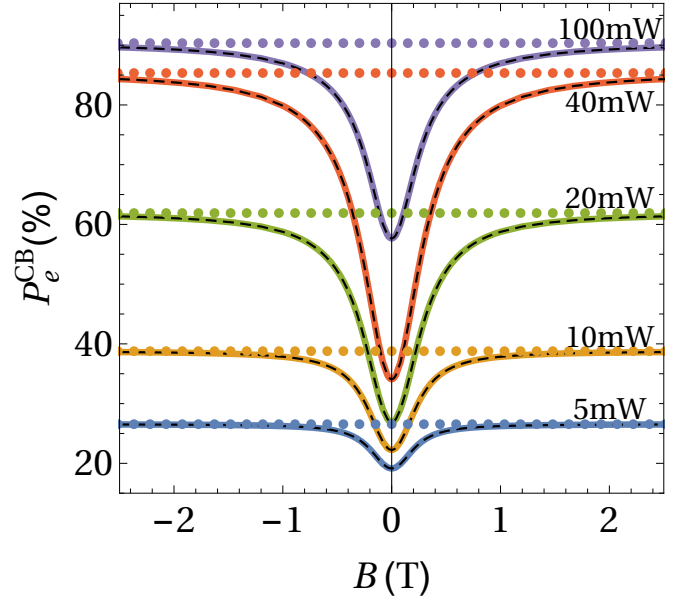


Figure 2.  $P_e^{CB}$  as a function of a magnetic field in the Faraday configuration for various powers  $W$  for the non-selective model. Results under  $\sigma^+$  (solid lines) and  $\sigma^-$  (dashed lines) light excitation are present. The nuclear spin relaxation times are  $\tau_{n1} = 5800$  ps and  $\tau_{n2} = 533$  ps. Dotted horizontal lines present the behaviour of polarization in the absence of NSR.

and (A7) in (A5) the dissipators for UTs and PTs are

$$\hat{\mathcal{D}}_1 = -\frac{1}{3\tau_{n1}} \sum_{i=1}^3 [\hat{I}_{1i}, [\hat{I}_{1i}, \hat{\rho}]], \quad (46)$$

$$\hat{\mathcal{D}}_2 = -\frac{1}{3\tau_{n2}} \sum_{i=1}^3 [\hat{I}_{2i}, [\hat{I}_{2i}, \hat{\rho}]], \quad (47)$$

where  $\hat{I}_{1i}$  and  $\hat{I}_{2i}$  are the  $i$ -th components of the nuclear spin operators' for UTs' and PTs' respectively. The NSR times for unpaired and paired traps are considered to be different in principle and therefore are set to  $\tau_{n1}$  and  $\tau_{n2}$ .

Finally we study the relaxation owing to the quadrupole interaction with random fluctuation of the local electric field gradient. The Hamiltonian takes the form of (A1) where  $k = 2$ . Substituting the rank  $k = 2$  irreducible spherical tensors in Eqs. (A8)-(A10) in terms of the nuclear angular momentum components in (A5) yield the following dissipators

$$\hat{\mathcal{D}}_1 = -\frac{1}{2\tau_{n1}} \sum_{i=1}^5 [\hat{Q}_{1,i}, [\hat{Q}_{1,i}, \hat{\rho}]], \quad (48)$$

$$\hat{\mathcal{D}}_2 = -\frac{1}{2\tau_{n2}} \sum_{i=1}^5 [\hat{Q}_{2,i}, [\hat{Q}_{2,i}, \hat{\rho}]]. \quad (49)$$

Here, the operators  $\hat{Q}_{1i}$  and  $\hat{Q}_{2i}$  are related to the rank  $k = 2$  irreducible spherical tensors and therefore can be

expressed in terms of the nuclear spin operators as

$$\hat{Q}_{n,1} = \frac{1}{2\sqrt{3}} \left( \hat{I}_{nx}^2 - \hat{I}_{ny}^2 \right), \quad (50)$$

$$\hat{Q}_{n,2} = \frac{1}{2\sqrt{3}} \left( \hat{I}_{nx}\hat{I}_{ny} + \hat{I}_{ny}\hat{I}_{nx} \right), \quad (51)$$

$$\hat{Q}_{n,3} = \frac{1}{2\sqrt{3}} \left( \hat{I}_{nx}\hat{I}_{nz} + \hat{I}_{nz}\hat{I}_{nx} \right), \quad (52)$$

$$\hat{Q}_{n,4} = \frac{1}{2\sqrt{3}} \left( \hat{I}_{ny}\hat{I}_{nz} + \hat{I}_{nz}\hat{I}_{ny} \right), \quad (53)$$

$$\hat{Q}_{n,5} = \frac{1}{6} \left( 2\hat{I}_{nz}^2 - \hat{I}_{ny}^2 - \hat{I}_{nx}^2 \right). \quad (54)$$

The explicit forms of the dissipators corresponding to the dipolar interaction (46)-(47) and quadrupole interaction (48)-(49) are presented in Appendix B.

### III. RESULTS AND DISCUSSION

The model developed above is used in this section to examine the interplay of the HFI and the NSR mechanisms in the continuous wave (CW) and pulsed excitation (PE) regimes. First, the theoretical results are compared with previous experimental observations under CW excitation in order to identify the main interaction behind NSR and HFI in Ga centers. Then, we analyze the dynamics of the bound electrons' and nuclear spin in the PE regime. We outline a method for detecting the bound electron and nuclear spin coherent oscillations induced by HFI by means of a pump-probe PL scheme.

In order to extract information from the model, we start by building the system of kinetic equations that follow from the master equation (2). By multiplying both sides of (2) by  $\hat{\lambda}_q$ , inserting the density matrix in the form (28) into the resulting expression and taking the trace we obtain a set of  $n = 85$  differential equations of the form

$$\begin{aligned} \dot{\lambda}_q &= \frac{i}{\hbar} \text{Tr} \left[ \left[ \hat{H}, \hat{\lambda}_q \right] \hat{\rho} \right] + \text{Tr} \left[ \mathcal{D} \hat{\lambda}_q \right] \\ &= F_q(\lambda_1, \lambda_2, \dots, \lambda_n, t), \quad q = 1, 2, \dots, n. \end{aligned} \quad (55)$$

Unlike the TCM that only considers the SDR mechanism, Zeeman interaction and electron spin relaxation, these new kinetic equations also take into account the HFI and NSR.

We study the spin dynamics of electrons and nuclei by numerically solving the system of ordinary differential equations (55). The relevant parameters are then extracted from the thus obtained  $\lambda_q$  functions which in turn are the quantum statistical averages. We assume that before the optical excitation ( $t = 0$ ) the UTs are equally populated and that the electrons as well as the nuclei are completely unpolarized. Therefore, initially  $N_1(0) = \lambda_6(0) = N_c$  and  $\lambda_q = 0$  for  $q \neq 6$ . Notice that these initial conditions also imply that at this stage there are no PTs, namely  $N_2(0) = \lambda_{70}(0) = 0$ .

#### A. Nuclear spin relaxation: CW regime

Under CW stimulation, the generation of spin up and spin down electrons is given by the smooth step function

$$G_{\uparrow\downarrow} = WG \frac{1 \pm P_i}{4} \left[ 1 + \tanh \left( \frac{t - t_0}{\sigma} \right) \right], \quad (56)$$

where  $W$  is the excitation power,  $G = 3.0 \times 10^{23} \text{ mW}^{-1} \text{ s}^{-1} \text{ cm}^{-3}$  is the power to generated electron ratio,  $P_i = \pm 0.15$  is the spin polarization degree of the optically generated CB electrons,  $t_0 = 100 \text{ ps}$  is the onset time of the excitation and  $\sigma = 10 \text{ ps}$  is the duration of the onset. The system is allowed to evolve for a sufficiently long time (200 ns) to reach steady state conditions.

Some of the parameters as  $N_c = 3 \times 10^{15} \text{ cm}^{-3}$ ,  $\tau_s = 150 \text{ ps}$ ,  $\tau_{sc} = 1500 \text{ ps}$ ,  $\tau^* = 1/c_n N_c = 2 \text{ ps}$ ,  $\tau_h^* = 1/c_p N_c = 30 \text{ ps}$ ,  $g = +1$  and  $g_c = +2$  where estimated from previous experimental results<sup>20,21,32,45</sup>. For the nuclei at the Ga centers, the hyperfine parameter was estimated to be  $A = 6.9 \times 10^{-2} \text{ cm}^{-1} = 8.5 \mu\text{eV}$ , the average hyperfine parameter of the two stable isotopes of Ga<sup>22,32,36</sup>. The NSR times  $\tau_{n1}$  and  $\tau_{n2}$  are determined below by comparing the theoretical calculations with the experimental results.

As we stated above, the two key features behind the HFI in Ga centers are a growth in the PL degree of circular polarization  $P_e^{CB}$ <sup>32,34-37</sup> and an Overhauser-like magnetic field<sup>32,33,35-37</sup>. Both are observed under circularly polarized excitation and a Faraday configuration magnetic field.

More specifically for the first feature,  $P_e^{CB}(B_z)$  exhibits a minimum close to  $B_z = 0$ . As  $|B_z|$  increases,  $P_e^{CB}$  saturates at values above  $B_z \approx 25 \text{ mT}$  where Zeeman energies are comparable to the HFI. In this region the HFI has been completely exceeded by the Zeeman interaction and therefore the bound electrons and nuclei in the Ga centers are effectively decoupled. The degree of circular polarization of the CB to VB photoluminescence as a function of the Faraday configuration magnetic field can be described by an inverted Lorentzian-like curve. In Fig. 2 we have calculated the CB electron spin polarization  $P_e^{CB} = 2S_z/n$  as a function of the magnetic field in Faraday configuration  $B_z$  under a circularly polarized excitation. In this case we have chosen the spin relaxation times  $\tau_{n1} = 5800 \text{ ps}$  and  $\tau_{n2} = 533 \text{ ps}$  that give good quantitative agreement with the experiment. The degree of the CB electron spin polarization as a function of the Faraday configuration magnetic field for the non-selective mechanism is shown in Fig. 2 for different pump powers  $W$ . As a reference, Fig. 2 also presents the behaviour observed in the absence of NSR ( $\mathcal{D}_1 = \mathcal{D}_2 = 0$ ) as thick dotted lines. These plots show that despite the HFI, in the absence of spin relaxation,  $P_e^{CB}(B_z)$  does not display any sign of the spin filtering enhancement. These results are exactly the same as those obtained with the TCM that does not contain the effects of the HFI. Therefore, in order for the effects of the HFI- as the amplification of the spin filtering effect-to be visible, NSR is essential.

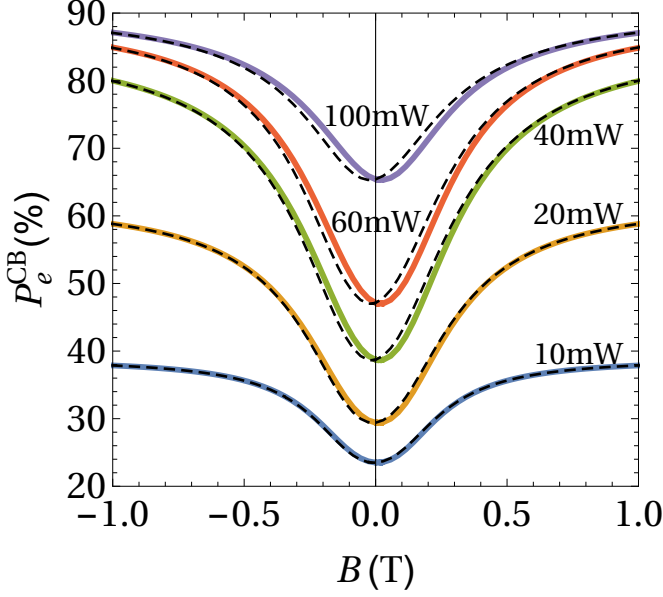


Figure 3.  $P_e^{CB}$  as a function of the magnetic field in the Faraday configuration for various powers  $W$  for the dipolar model. Results under  $\sigma^+$  (solid lines) and  $\sigma^-$  (dashed lines) light excitation are shown.

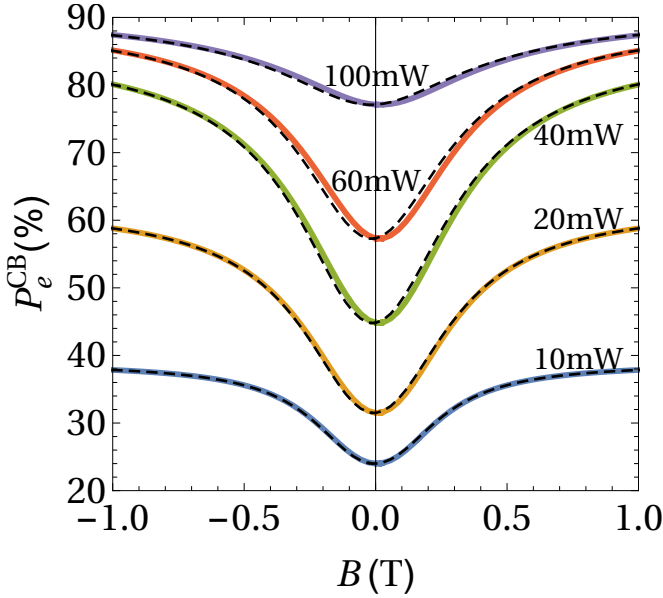


Figure 4.  $P_e^{CB}$  as a function of the magnetic field in the Faraday configuration for various powers  $W$  for the quadrupolar model. Results under  $\sigma^+$  (solid lines) and  $\sigma^-$  (dashed lines) light excitation are presented.

The second feature of this phenomenon is a shift of the minimum of  $P_e^{CB}$  vs.  $B_z$  that points to the existence of an Overhauser-like magnetic field<sup>33</sup>. The  $P_e^{CB}(B_z)$  curves are shifted to the positive and negative magnetic field regions depending on the helicity of the circularly polarized light. Thereby, under  $\sigma^-$  and  $\sigma^+$  excitation the

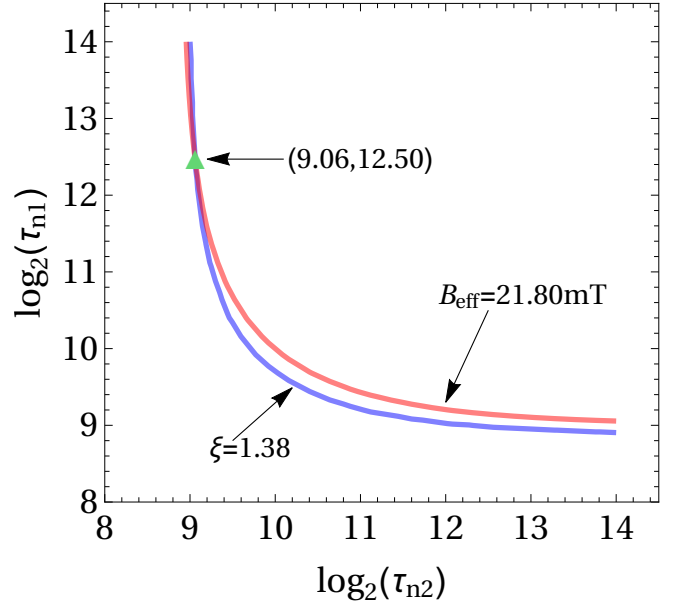


Figure 5. Isolines of the Overhauser-like magnetic field  $B_{\text{eff}}$  and depth  $\xi = P_e^{CB}(\infty)/P_e^{CB}(0)$  at fixed power for the dipolar relaxation mechanism. The isolines for  $B_{\text{eff}} = 21.8$  mT and  $\xi = 1.38$  under an excitation power of  $W = 100$  mW are shown. These two lines cross at the point marked with the (green) triangle in  $\tau_{n1} = 5800$  ps and  $\tau_{n2} = 533$  ps.

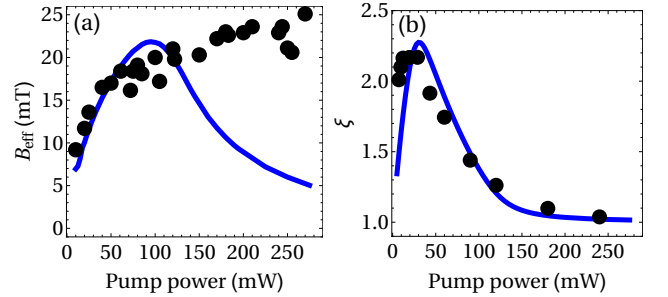


Figure 6. Overhauser-like magnetic field  $B_{\text{eff}}$  (a) and  $\xi$  (b) as functions of the excitation power  $W$  for the dipolar nuclear spin relaxation mechanism. In inset (a), the experimental data (solid circles) present the shift of the intensity dependence  $J(B_z)$  while the simulated curve (solid lines) is obtained for the electron polarization dependence  $P_e^{CB}(B_z)$ . Inset (b) shows the experimental (solid circles)<sup>32,37</sup> and theoretical (solid line) results for  $\xi$ .

minimum is located at  $B_z = B_{\text{eff}} < 0$  and  $B_z = B_{\text{eff}} > 0$  respectively. The experimental data shows that  $B_{\text{eff}}$  grows with the excitation power  $W$  until it apparently saturates at approximately 25 mT. The non-selective dissipator yields vanishing  $B_{\text{eff}}$  as no shift is observed for  $P_e^{CB}$  in Fig. 2. This dissipator is too symmetric to be able to produce an Overhauser-like magnetic field and hence must be ruled out as the leading NSR mechanism.

In contrast, the dipolar and quadrupolar mechanisms yield non-vanishing  $B_{\text{eff}}$  as it can be seen in Figs. 3 and 4. These two plots show  $P_e^{CB}(B_z)$  for the dipolar



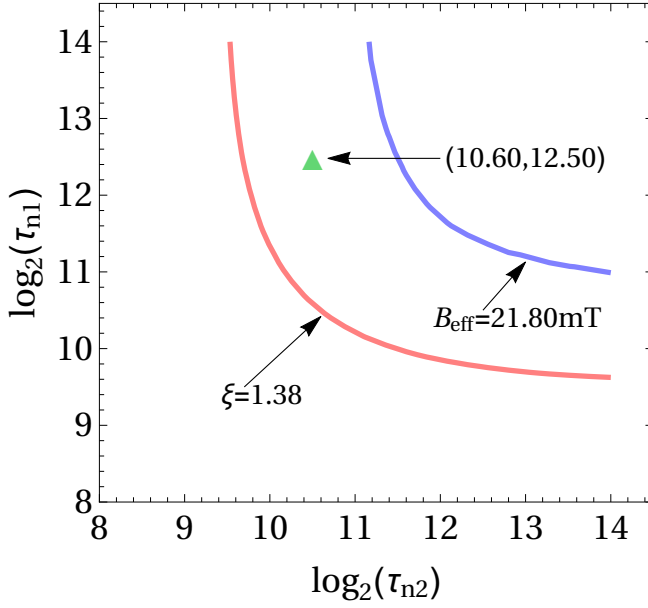


Figure 7. Isolines of the Overhauser-like magnetic field  $B_{\text{eff}}$  and depth  $\xi = P_e^{CB}(\infty)/P_e^{CB}(0)$  at fixed power for the quadrupolar relaxation mechanism. The isolines for  $B_{\text{eff}} = 21.80 \text{ mT}$  and  $\xi = 1.38$  under an excitation power of  $W = 100 \text{ mW}$  are shown. Even though these two lines do not cross we have marked with a (green) triangle the point  $\tau_{n1} = 5800 \text{ ps}$  and  $\tau_{n2} = 1550 \text{ ps}$  that yield the best fit.

and quadrupolar dissipators for various excitation powers. Even though the shifts produced by both mechanisms qualitatively agree with the experimental observations, only the dipolar one is able to accurately fit the experimental measurements as we discuss below. In addition to the Overhauser-like magnetic field, another feature that strongly depends on the NSR mechanism is the depth of the inverted Lorentzian-like  $P_e^{CB}(B_z)$  curves given by  $\xi = P_e^{CB}(\infty)/P_e^{CB}(0)$ . To discern which of the two mechanisms is the dominant one, we compare our theoretical calculations with the experimental observations of  $B_{\text{eff}}$  and  $\xi$ <sup>32,33,37</sup>. The power dependence of  $B_{\text{eff}}$  and  $\xi$  is determined by finding the minima  $P_e^{CB}(0)$  and maxima  $P_e^{CB}(\infty)$  of  $P_e^{CB}(B_z)$  for different excitation powers.

In Fig. 5 we plot the isolines for  $B_{\text{eff}} = 21.8 \text{ mT}$  and  $\xi = 1.38$  as functions of the NSR times  $\tau_{n1}$  and  $\tau_{n2}$ . These two correspond to the experimental results observed for an excitation power of  $W = 100 \text{ mW}$ <sup>32</sup>. The two isolines intersect at  $\tau_{n1} = 5800 \text{ ps}$  and  $\tau_{n2} = 533 \text{ ps}$ . In accordance with these results, the  $B_{\text{eff}}$  and  $\xi$  isolines at other excitation power coincide at similar  $\tau_{n1}$  and  $\tau_{n2}$  values. Collecting the intersecting points of all the experimental results we find that the NSR times must fall within the ranges  $5800 \text{ ps} < \tau_{n1} < 8100 \text{ ps}$  and  $500 \text{ ps} < \tau_{n2} < 700 \text{ ps}$ . Plots of  $B_{\text{eff}}$  and  $\xi$  as functions of the excitation power are shown in Figs. 6 (a) and 6(b) respectively. The best quantitative agreement with the experimental data is accomplished by using the NSR times

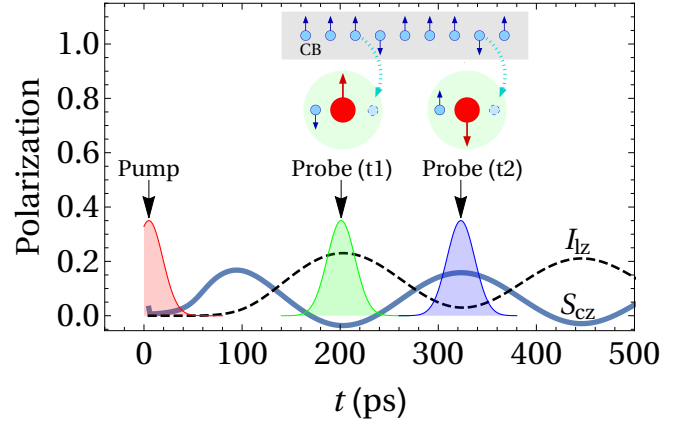


Figure 8. Time dependence of the spin polarization of bound electrons  $S_{cz}$  (solid lines) and nuclei  $I_{1z}$  (dashed lines) after being excited by the pump pulse. The pump pulse is left circularly polarized and therefore the majority of the electrons are spin polarized in the  $+z$  direction. Two extreme situations are illustrated. In the probe pulse 1 bound electrons are spin polarized in the same direction as CB electrons and in the probe pulse 2 bound electrons are spin polarized in the opposite direction to CB electrons. In the first situation CB electrons with the opposite spin polarization to the majority are rapidly recombined through the Ga centers enhancing the spin filtering effect. In this case a large  $SDR_r$  is expected. In contrast, in the second situation, CB electrons whose spin polarization is that of the majority are efficiently recombined lowering the  $SDR_r$ .

$\tau_{n1} = 5800 \text{ ps}$  and  $\tau_{n2} = 533 \text{ ps}$  consistent with the ranges above. Whereas the calculated  $\xi$  presents a very good agreement with the experimental data, the theoretical values of  $B_{\text{eff}}$  above  $100 \text{ mW}$  show a significant deviation with respect to the experimental observations. The experimental results suggest that after increasing with the excitation power,  $B_{\text{eff}}$  saturates at approximately  $25 \text{ mT}$ . However, the computed  $B_{\text{eff}}$  as a function of the excitation vanishes for high powers after reaching its maximum at  $25 \text{ mT}$  (see Fig. 6).

The quadrupolar mechanism, however, yields systematically non-intersecting isolines regardless of the excitation power value used to calculate them. In Fig. 7 we present the  $B_{\text{eff}} = 21.8 \text{ mT}$  and  $\xi = 1.38$  isolines that clearly do not intersect. This behaviour is observed for all the excitation powers reported experimentally and therefore we must also rule out the quadrupolar mechanism.

## B. Coherent oscillations of electronic and nuclear spins in Ga centers: PE regime

Having identified the NSR mechanism and the corresponding relaxation times we are in a position to consider time resolved simulations. Our aim here is to develop a method to observe the coherent oscillations of bound electrons and nuclei in Ga centers. To do so we propose a pump probe scheme that we describe below.

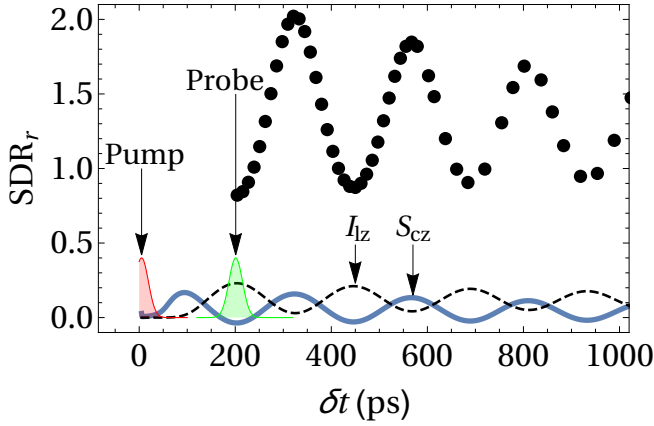


Figure 9. Trace of the coherent electron-nuclear spin oscillations via the  $SDR_r$ . The solid circles correspond to maxima of the time resolved  $SDR_r$  as a function of the time delay  $\delta t$  between the pump and the probe pulses. Below,  $S_{cz}$  (solid line) and  $I_{1z}$  (dashed line) are presented for reference.

In PE regime, the generation terms are given by

$$G_{\uparrow\downarrow} = \frac{TWG}{\sigma\sqrt{2\pi}} \frac{1 \pm P_i}{2} \left[ e^{-\frac{t^2}{2\sigma^2}} + \eta e^{-\frac{(t-\delta t)^2}{2\sigma^2}} \right], \quad (57)$$

where  $W$  is the pulse's average power,  $\sigma = 1$  ps is its width and  $T = 12$  ns is the period between repeated pulses<sup>31</sup>. The pump pulse originates at  $t = 0$  and the probe is delayed  $\delta t$ .

Figure 8 is an outline of the proposed method. The pump pulse is left circularly polarized and therefore most of the electrons are spin polarized in the  $+z$  direction. Likewise, the probe pulses are left circularly polarized. Fig. 8 also shows a plot of the bound electron and nuclear spin polarizations as a function of time after being excited by the pump pulse. The pump and probe pulse widths are exaggerated to make them visible in the given time scale. In this plot it is possible to observe the electron-nucleus flip-flops as oscillations of  $I_{1z}$  (dashed lines) and  $S_{cz}$  (thick lines) that are phase shifted by  $\pi/2$ . As indicated in this diagram, the second pulse at time delays  $t_1$  and  $t_2$  probes two extreme situations. In the first one CB electron and bound electrons are mostly spin polarized in opposite directions. The center is therefore more likely to capture a CB electron whose spin is oriented in the opposite direction to the majority therefore rising the population of electrons in the CB. In contrast, in the second situation centers are more likely to capture electrons whose direction is parallel to the majority diminishing the electron population in the CB. A good estimate of the electron and hole population in either situation is the time resolved SDR ratio given by

$$SDR_r(t) = \frac{I_+}{I_X} = \frac{n_{\sigma_+}(t)p_{\sigma_+}(t)}{n_{\pi_X}(t)p_{\pi_X}(t)}, \quad (58)$$

where the PL intensity under circularly polarized light  $I_+ \propto n_{\sigma_+}(t)p_{\sigma_+}(t)$  is proportional to the CB and VB

density populations  $n_{\sigma_+}(t)$  and  $p_{\sigma_+}(t)$ . Similarly  $I_X \propto n_{\pi_X}(t)p_{\pi_X}(t)$  where  $n_{\pi_X}(t)$  and  $p_{\pi_X}(t)$  are the density populations of CB electrons and holes under linearly polarized light. If CB electrons are captured spin dependently by the Ga centers then  $n_{\sigma_+}(t) > n_{\pi_X}(t)$  and  $p_{\sigma_+}(t) > p_{\pi_X}(t)$  and therefore  $SDR_r > 1$ . In accordance with the above considerations,  $SDR_r(\delta t_1) > SDR_r(\delta t) > SDR_r(\delta t_2)$  where  $\delta t_1 < \delta t < \delta t_2$ . Thus, it is possible to trace the oscillations of bound electrons and nuclei by successively measuring the time resolved  $SDR_r$  for different probe pulse delays.

By determining the maxima of the time resolved  $SDR_r$  for different probe pulse delays we have obtained the plot displayed in Fig. 9 setting  $\eta=1$ . Here the  $SDR_r$  maxima are plotted as a function of their corresponding time delays  $\delta t$  as closed circles. Similar results (not shown here) are obtained by calculating the  $SDR_r$  from the integrated PL. Below, the spin polarization of bound electrons  $S_{cz}$  and nuclear spin polarization  $I_{1z}$  are shown for reference. This plots demonstrate that it is possible to trace the coherent oscillations of the spin polarization of bound electrons interacting with the nuclei by means of the time resolved  $SDR$  ratio.

#### IV. SUMMARY

We have analyzed the spin dynamics of electrons and nuclei in GaAsN by developing a model based on the master equation approach. The main mechanisms behind the spin dependent recombination are considered as well as the hyperfine interaction in Ga paramagnetic traps. We have demonstrated that the NSR in centers plays an essential role in reproducing the two most significant signatures of the HFI in Ga centers. First, the amplification of the spin filtering effect under a Faraday configuration magnetic field is visible only if some NSR mechanism is present. Second, the features of the Overhauser-like magnetic field not only depend on the HFI but also strongly rely on the nature of the NSR mechanism. We have tested the dipolar interaction between neighbouring Ga atoms and the quadrupolar interaction of Ga centers with random charge distribution background. We have proven that the dipolar is the only mechanism compatible with the experimental observations. Indeed, a scenario where large charge distribution variations are present in the vicinity of the Ga nuclei is difficult to imagine. Although most of the experimental results are correctly reproduced by our model some of the aspects regarding the behaviour of the Overhauser-like magnetic field remain elusive. One of these is the discrepancy between the saturation values in the high power regime. This is important since it would allow to pinpoint the exact origin of the NSR mechanism.

To further explore the effects of the HFI and the NSR we have tested the model in the PE regime. In particular, we have proposed a pump-probe scheme that allows to trace the coherent oscillations of the bound electron spin

interacting with its nucleus through the HFI.

Even though in principle this model is conceived for Ga centers, it can be easily adapted for other type of centers where dipolar or quadrupolar interactions play an important role as the leading mechanisms of NSR.

## ACKNOWLEDGMENTS

French and Russian authors acknowledge funding from LIA CNRS-Ioffe RAS ILNACS. L.A.B., V.K.K. and E.L.I. acknowledge the Russian Foundation for Basic Research (Grant No. 14-02-00959). A.K. gratefully appreciates the financial support of “Departamento de Ciencias Básicas UAM-A” grant numbers 2232214 and 2232215. J.C.S.S. and V.G.I.S. would like to acknowledge the support received from the “Becas de Posgrado UAM” scholarship numbers 2151800745 and 2112800069. We are indebted to Professor J. Grabinsky for the careful reading of the manuscript.

## Appendix A: Redfield relaxation theory

According to the Wangsness, Bloch, and Redfield relaxation theory<sup>38–41</sup> the interaction of a nucleus with its surroundings can be accounted for by the Hamiltonian

$$\hat{\mathcal{H}}(t) = \gamma \sum_{r=-k}^k f_{k,r}^*(t) \hat{\mathbf{T}}_{k,r}, \quad (\text{A1})$$

where  $\gamma$  is a constant,  $\hat{\mathbf{T}}_{k,r}$  is a  $r$ -th component of the rank  $k$  irreducible spherical tensor and  $f_{k,r}(t)$  is a random function that describes the interaction with the surroundings.

To second-order, the average fluctuations of the surroundings with the nucleus are given by the following dissipator

$$\hat{\mathcal{D}} = -\frac{1}{\hbar^2} \int_{-\infty}^t dt' \overline{\left[ \hat{\mathcal{H}}(t), \left[ \hat{\mathcal{H}}(t'), \bar{\hat{\rho}} \right] \right]}, \quad (\text{A2})$$

where  $\bar{\hat{\rho}}$  is the average density matrix. By substituting the Hamiltonian (A1) in (A2) and using the fact that  $f_{k,r}^*(t) = (-1)^r f_{k,-r}(t)$  and  $\hat{\mathbf{T}}_{k,r}^\dagger = (-1)^r \hat{\mathbf{T}}_{k,-r}$  we get the general form of the dissipator

$$\begin{aligned} \hat{\mathcal{D}} = & -\frac{1}{\hbar^2} \sum_{s,r=-k}^k \left[ \hat{\mathbf{T}}_{k,s}^\dagger, \left[ \hat{\mathbf{T}}_{k,r}, \bar{\hat{\rho}} \right] \right] \\ & \times \left( \int_{-\infty}^t dt' \overline{f_{k,s}(t) f_{k,r}^*(t')} \right). \quad (\text{A3}) \end{aligned}$$

The above dissipator describes the interaction of a nucleus with the fluctuations of a random electromagnetic field. The functions  $f_{k,s}(t)$  and  $f_{k,r}^*(t')$  comply with

$$\overline{f_{k,s}(t) f_{k,r}^*(t')} = \delta_{s,r} \xi e^{-|t-t'|/\tau}, \quad (\text{A4})$$

where  $\xi e^{-|t-t'|/\tau}$  is a correlation function.  $\tau$  is the correlation time of the fluctuating field and  $\xi$  is the correlation amplitude when  $t = t'$ . With (A4), the dissipator  $\hat{\mathcal{D}}$  (A3) is simplified to

$$\hat{\mathcal{D}}_{\text{NSR}} = -\frac{1}{2\tau_n} \sum_{r=-k}^k \left[ \hat{\mathbf{T}}_{k,r}^\dagger, \left[ \hat{\mathbf{T}}_{k,r}, \bar{\hat{\rho}} \right] \right], \quad (\text{A5})$$

where  $\tau_n = \hbar^2/2\xi\tau$  is the NSR time.

In the case of magnetic dipole interactions, only the irreducible spherical tensors of rank  $k = 1$  participate in the Hamiltonian (A1). They can be expressed in terms of the nuclear spin components as

$$\hat{\mathbf{T}}_{1,0} = \hat{I}_z, \quad (\text{A6})$$

$$\hat{\mathbf{T}}_{1,\pm 1} = \mp \frac{1}{\sqrt{2}} (\hat{I}_x \pm i\hat{I}_y), \quad (\text{A7})$$

and for electric quadrupole interaction the rank is  $k = 2$  and their components are

$$\hat{\mathbf{T}}_{2,0} = \frac{1}{6} [2\hat{I}_z^2 - \hat{I}_y^2 - \hat{I}_x^2], \quad (\text{A8})$$

$$\hat{\mathbf{T}}_{2,\pm 1} = \mp \frac{1}{2\sqrt{6}} [\hat{I}_x \hat{I}_z + \hat{I}_z \hat{I}_x \pm i(\hat{I}_y \hat{I}_z + \hat{I}_z \hat{I}_y)], \quad (\text{A9})$$

$$\hat{\mathbf{T}}_{2,\pm 2} = \frac{1}{2\sqrt{6}} [(\hat{I}_x^2 - \hat{I}_y^2) \pm i(\hat{I}_x \hat{I}_y + \hat{I}_y \hat{I}_x)]. \quad (\text{A10})$$

## Appendix B: Explicit form of the dipolar and quadrupolar interactions

The quadrupolar dissipator for PT is given explicitly by

$$(\hat{\mathcal{D}}_2)_{\frac{3}{2}, \frac{3}{2}} = -\frac{1}{\tau_{n2}} \left( \rho_{2;\frac{3}{2}, \frac{3}{2}} - \frac{\rho_{2;\frac{1}{2}, \frac{1}{2}} + \rho_{2;-\frac{1}{2}, -\frac{1}{2}}}{2} \right), \quad (\text{B1})$$

$$(\hat{\mathcal{D}}_2)_{-\frac{3}{2}, -\frac{3}{2}} = -\frac{1}{\tau_{n2}} \left( \rho_{2;-\frac{3}{2}, -\frac{3}{2}} - \frac{\rho_{2;\frac{1}{2}, \frac{1}{2}} + \rho_{2;-\frac{1}{2}, -\frac{1}{2}}}{2} \right), \quad (\text{B2})$$

$$(\hat{\mathcal{D}}_2)_{\frac{1}{2}, \frac{1}{2}} = -\frac{1}{\tau_{n2}} \left( \rho_{2;\frac{1}{2}, \frac{1}{2}} - \frac{\rho_{2;\frac{3}{2}, \frac{3}{2}} + \rho_{2;-\frac{3}{2}, -\frac{3}{2}}}{2} \right), \quad (\text{B3})$$

$$(\hat{\mathcal{D}}_2)_{-\frac{1}{2}, -\frac{1}{2}} = -\frac{1}{\tau_{n2}} \left( \rho_{2;-\frac{1}{2}, -\frac{1}{2}} - \frac{\rho_{2;\frac{3}{2}, \frac{3}{2}} + \rho_{2;-\frac{3}{2}, -\frac{3}{2}}}{2} \right), \quad (\text{B4})$$

$$(\hat{\mathcal{D}}_2)_{\frac{3}{2}, \frac{1}{2}} = -\frac{1}{2\tau_{n2}} (3\rho_{2;\frac{3}{2}, \frac{1}{2}} - \rho_{2;-\frac{1}{2}, -\frac{3}{2}}), \quad (\text{B5})$$

$$(\hat{\mathcal{D}}_2)_{-\frac{3}{2}, -\frac{1}{2}} = -\frac{1}{2\tau_{n2}} (3\rho_{2;-\frac{3}{2}, -\frac{1}{2}} - \rho_{2;\frac{1}{2}, \frac{3}{2}}), \quad (\text{B6})$$

$$(\hat{\mathcal{D}}_2)_{-\frac{1}{2}, -\frac{3}{2}} = -\frac{1}{2\tau_{n2}} (3\rho_{2;-\frac{1}{2}, -\frac{3}{2}} - \rho_{2;\frac{3}{2}, \frac{1}{2}}), \quad (\text{B7})$$

$$(\hat{\mathcal{D}}_2)_{\frac{1}{2}, \frac{3}{2}} = -\frac{1}{2\tau_{n2}} (3\rho_{2;\frac{1}{2}, \frac{3}{2}} - \rho_{2;-\frac{3}{2}, -\frac{1}{2}}), \quad (\text{B8})$$

$$(\hat{\mathcal{D}}_2)_{\frac{1}{2}, -\frac{1}{2}} = -\frac{1}{\tau_{n2}} \rho_{2;\frac{1}{2}, -\frac{1}{2}}, \quad (\text{B9})$$

$$(\hat{\mathcal{D}}_2)_{-\frac{1}{2}, \frac{1}{2}} = -\frac{1}{\tau_{n2}} \rho_{2;-\frac{1}{2}, \frac{1}{2}}, \quad (\text{B10})$$

$$(\hat{\mathcal{D}}_2)_{\frac{3}{2}, -\frac{1}{2}} = -\frac{1}{2\tau_{n2}} \left( 3\rho_{2;\frac{3}{2}, -\frac{1}{2}} + \rho_{2;\frac{1}{2}, -\frac{3}{2}} \right), \quad (\text{B11})$$

$$(\hat{\mathcal{D}}_2)_{\frac{1}{2}, -\frac{3}{2}} = -\frac{1}{2\tau_{n2}} \left( 3\rho_{2;\frac{1}{2}, -\frac{3}{2}} + \rho_{2;\frac{3}{2}, -\frac{1}{2}} \right), \quad (\text{B12})$$

$$(\hat{\mathcal{D}}_2)_{-\frac{3}{2}, \frac{1}{2}} = -\frac{1}{2\tau_{n2}} \left( 3\rho_{2;-\frac{3}{2}, \frac{1}{2}} + \rho_{2;-\frac{1}{2}, \frac{3}{2}} \right), \quad (\text{B13})$$

$$(\hat{\mathcal{D}}_2)_{-\frac{1}{2}, \frac{3}{2}} = -\frac{1}{2\tau_{n2}} \left( 3\rho_{2;-\frac{1}{2}, \frac{3}{2}} + \rho_{2;-\frac{3}{2}, \frac{1}{2}} \right), \quad (\text{B14})$$

$$(\hat{\mathcal{D}}_2)_{\frac{3}{2}, -\frac{3}{2}} = -\frac{1}{\tau_{n2}} \rho_{2;\frac{3}{2}, -\frac{3}{2}}, \quad (\text{B15})$$

$$(\hat{\mathcal{D}}_2)_{-\frac{3}{2}, \frac{3}{2}} = -\frac{1}{\tau_{n2}} \rho_{2;-\frac{3}{2}, \frac{3}{2}}. \quad (\text{B16})$$

In a short form the above equations can be presented as

$$(\hat{\mathcal{D}}_2)_{m, m'} = -\frac{1}{\tau_{n2}} \sum_{m_1, m'_1} Q_{m, m'; m_1, m'_1}^{(\text{EQ})} \rho_{2; m_1, m'_1}.$$

Then the quadrupolar dissipator for UT is given by

$$(\hat{\mathcal{D}}_1)_{s, m; s', m'} = -\frac{1}{\tau_{n1}} \sum_{m_1, m'_1} Q_{m, m'; m_1, m'_1}^{(\text{EQ})} \rho_{1; s, m_1; s', m'_1}.$$

The dipolar dissipator for PTs is given explicitly by

$$(\hat{\mathcal{D}}_2)_{\frac{3}{2}, \frac{3}{2}} = -\frac{1}{\tau_{n2}} \left( \rho_{2;\frac{3}{2}, \frac{3}{2}} - \rho_{2;\frac{1}{2}, \frac{1}{2}} \right), \quad (\text{B17})$$

$$(\hat{\mathcal{D}}_2)_{-\frac{3}{2}, -\frac{3}{2}} = -\frac{1}{\tau_{n2}} \left( \rho_{2;-\frac{3}{2}, -\frac{3}{2}} - \rho_{2;-\frac{1}{2}, -\frac{1}{2}} \right), \quad (\text{B18})$$

$$(\hat{\mathcal{D}}_2)_{\frac{1}{2}, \frac{1}{2}} = -\frac{1}{3\tau_{n2}} \left( 7\rho_{2;\frac{1}{2}, \frac{1}{2}} - 3\rho_{2;\frac{3}{2}, \frac{3}{2}} - 4\rho_{2;-\frac{1}{2}, -\frac{1}{2}} \right), \quad (\text{B19})$$

$$(\hat{\mathcal{D}}_2)_{-\frac{1}{2}, -\frac{1}{2}} = -\frac{1}{3\tau_{n2}} \left( 7\rho_{2;-\frac{1}{2}, -\frac{1}{2}} - 3\rho_{2;-\frac{3}{2}, -\frac{3}{2}} - 4\rho_{2;\frac{1}{2}, \frac{1}{2}} \right), \quad (\text{B20})$$

$$(\hat{\mathcal{D}}_2)_{\frac{3}{2}, \frac{1}{2}} = -\frac{2}{3\tau_{n2}} \left( 3\rho_{2;\frac{3}{2}, \frac{1}{2}} - \sqrt{3}\rho_{2;\frac{1}{2}, -\frac{1}{2}} \right), \quad (\text{B21})$$

$$(\hat{\mathcal{D}}_2)_{\frac{1}{2}, -\frac{1}{2}} = -\frac{2}{3\tau_{n2}} \left[ 4\rho_{2;\frac{1}{2}, -\frac{1}{2}} - \sqrt{3} \left( \rho_{2;\frac{3}{2}, \frac{1}{2}} + \rho_{2;-\frac{1}{2}, -\frac{3}{2}} \right) \right], \quad (\text{B22})$$

$$(\hat{\mathcal{D}}_2)_{-\frac{1}{2}, -\frac{3}{2}} = -\frac{2}{3\tau_{n2}} \left( 3\rho_{2;-\frac{1}{2}, -\frac{3}{2}} - \sqrt{3}\rho_{2;\frac{1}{2}, -\frac{1}{2}} \right), \quad (\text{B23})$$

$$(\hat{\mathcal{D}}_2)_{\frac{1}{2}, \frac{3}{2}} = -\frac{2}{3\tau_{n2}} \left( 3\rho_{2;\frac{1}{2}, \frac{3}{2}} - \sqrt{3}\rho_{2;-\frac{1}{2}, \frac{1}{2}} \right), \quad (\text{B24})$$

$$(\hat{\mathcal{D}}_2)_{-\frac{1}{2}, \frac{1}{2}} = -\frac{2}{3\tau_{n2}} \left[ 4\rho_{2;-\frac{1}{2}, \frac{1}{2}} - \sqrt{3} \left( \rho_{2;\frac{1}{2}, \frac{3}{2}} + \rho_{2;-\frac{3}{2}, -\frac{1}{2}} \right) \right], \quad (\text{B25})$$

$$(\hat{\mathcal{D}}_2)_{-\frac{3}{2}, -\frac{1}{2}} = -\frac{2}{3\tau_{n2}} \left( 3\rho_{2;-\frac{3}{2}, -\frac{1}{2}} - \sqrt{3}\rho_{2;-\frac{1}{2}, \frac{1}{2}} \right), \quad (\text{B26})$$

$$(\hat{\mathcal{D}}_2)_{\frac{3}{2}, -\frac{1}{2}} = -\frac{1}{\tau_{n2}} \left( 3\rho_{2;\frac{3}{2}, -\frac{1}{2}} - \rho_{2;\frac{1}{2}, -\frac{3}{2}} \right), \quad (\text{B27})$$

$$(\hat{\mathcal{D}}_2)_{\frac{1}{2}, -\frac{3}{2}} = -\frac{1}{\tau_{n2}} \left( 3\rho_{2;\frac{1}{2}, -\frac{3}{2}} - \rho_{2;\frac{3}{2}, -\frac{1}{2}} \right), \quad (\text{B28})$$

$$(\hat{\mathcal{D}}_2)_{-\frac{3}{2}, \frac{1}{2}} = -\frac{1}{\tau_{n2}} \left( 3\rho_{2;-\frac{3}{2}, \frac{1}{2}} - \rho_{2;-\frac{1}{2}, \frac{3}{2}} \right), \quad (\text{B29})$$

$$(\hat{\mathcal{D}}_2)_{-\frac{1}{2}, \frac{3}{2}} = -\frac{1}{\tau_{n2}} \left( 3\rho_{2;-\frac{1}{2}, \frac{3}{2}} - \rho_{2;-\frac{3}{2}, \frac{1}{2}} \right), \quad (\text{B30})$$

$$(\hat{\mathcal{D}}_2)_{\frac{3}{2}, -\frac{3}{2}} = -\frac{4}{\tau_{n2}} \rho_{2;\frac{3}{2}, -\frac{3}{2}}, \quad (\text{B31})$$

$$(\hat{\mathcal{D}}_2)_{-\frac{3}{2}, \frac{3}{2}} = -\frac{4}{\tau_{n2}} \rho_{2;-\frac{3}{2}, \frac{3}{2}}. \quad (\text{B32})$$

If the above equations are presented as

$$(\hat{\mathcal{D}}_2)_{m, m'} = -\frac{1}{\tau_{n2}} \sum_{m_1, m'_1} Q_{m, m'; m_1, m'_1}^{(\text{MD})} \rho_{2; m_1, m'_1},$$

then the depolar dissipator for UT is given by

$$(\hat{\mathcal{D}}_1)_{s, m; s', m'} = -\frac{1}{\tau_{n1}} \sum_{m_1, m'_1} Q_{m, m'; m_1, m'_1}^{(\text{MD})} \rho_{1; s, m_1; s', m'_1}.$$

- <sup>1</sup> A. Auer and G. Burkard, Phys. Rev. B **93**, 035402 (2016).
- <sup>2</sup> T. van der Sar, Z. H. Wang, M. S. Blok, H. Bernien, T. H. Taminiau, D. M. Toyli, D. A. Lidar, D. D. Awschalom, R. Hanson, and V. V. Dobrovitski, Nature **484**, 82 (2012).
- <sup>3</sup> N. Mizuochi, P. Neumann, F. Rempp, J. Beck, V. Jacques, P. Siyushev, K. Nakamura, D. J. Twitchen, H. Watanabe, S. Yamasaki, F. Jelezko, and J. Wrachtrup, Phys. Rev. B **80**, 041201 (2009).
- <sup>4</sup> J. R. Maze, J. M. Taylor, and M. D. Lukin, Phys. Rev. B **78**, 094303 (2008).
- <sup>5</sup> J. J. Pla, F. A. Mohiyaddin, K. Y. Tan, J. P. Dehollain, R. Rahman, G. Klimeck, D. N. Jamieson, A. S. Dzurak, and A. Morello, Phys. Rev. Lett. **113**, 246801 (2014).
- <sup>6</sup> B. E. Kane, Nature **393**, 133 (1998).
- <sup>7</sup> J. J. Pla, K. Y. Tan, J. P. Dehollain, W. H. Lim, J. J. L. Morton, D. N. Jamieson, A. S. Dzurak, and A. Morello, Nature **489**, 541 (2012).
- <sup>8</sup> T. D. Ladd, D. Maryenko, Y. Yamamoto, E. Abe, and K. M. Itoh, Phys. Rev. B **71**, 014401 (2005).
- <sup>9</sup> A. Laucht, R. Kalra, J. T. Muhonen, J. P. Dehollain, F. A. Mohiyaddin, F. Hudson, J. C. McCallum, D. N. Jamieson, A. S. Dzurak, and A. Morello, Appl. Phys. Lett. **104**, 092115 (2014), <http://dx.doi.org/10.1063/1.4867905>.
- <sup>10</sup> W. Yao, R.-B. Liu, and L. J. Sham, Phys. Rev. B **74**, 195301 (2006).
- <sup>11</sup> V. Ivády, K. Szász, A. L. Falk, P. V. Klimov, D. J. Christle, E. Janzén, I. A. Abrikosov, D. D. Awschalom, and A. Gali, Phys. Rev. B **92**, 115206 (2015).
- <sup>12</sup> T. D. Ladd, F. Jelezko, R. Laflamme, Y. Nakamura, C. Monroe, and J. L. O'Brien, Nature **464**, 45 (2010).
- <sup>13</sup> J. Wrachtrup, S. Yang, and D. D. B. Rao, SPIE Newsroom (2016), 10.1117/2.1201607.006539.
- <sup>14</sup> W. M. Witzel, M. S. Carroll, A. Morello, L. Cywiński, and S. Das Sarma, Phys. Rev. Lett. **105**, 187602 (2010).
- <sup>15</sup> R. Hanson, V. V. Dobrovitski, A. E. Feiguin, O. Gywat, and D. D. Awschalom, Science **320**, 352 (2008), <http://science.sciencemag.org/content/320/5874/352.full.pdf>.
- <sup>16</sup> D. Simin, V. A. Soltamov, A. V. Poshakinskiy, A. N. Anisimov, R. A. Babunts, D. O. Tolmachev, E. N. Mokhov, M. Trupke, S. A. Tarasenko, A. Sperlich, P. G. Baranov, V. Dyakonov, and G. V. Astakhov, Phys. Rev. X **6**, 031014 (2016).
- <sup>17</sup> J. J. Pla, K. Y. Tan, J. P. Dehollain, W. H. Lim, J. J. L. Morton, F. A. Zwanenburg, D. N. Jamieson, A. S. Dzurak, and A. Morello, Nature **496**, 334 (2013).
- <sup>18</sup> P.-F. Braun, X. Marie, L. Lombez, B. Urbaszek, T. Amand, P. Renucci, V. K. Kalevich, K. V. Kavokin, O. Krebs, P. Voisin, and Y. Masumoto, Phys. Rev. Lett. **94**, 116601 (2005).
- <sup>19</sup> E. Abe, A. M. Tyryshkin, S. Tojo, J. J. L. Morton, W. M. Witzel, A. Fujimoto, J. W. Ager, E. E. Haller, J. Isoya, S. A. Lyon, M. L. W. Thewalt, and K. M. Itoh, Phys. Rev. B **82**, 121201 (2010).
- <sup>20</sup> V. K. Kalevich, E. L. Ivchenko, M. M. Afanasiev, A. Y. Shiryaev, A. Y. Egorov, V. M. Ustinov, B. Pal, and Y. Masumoto, JETP Lett. **82**, 455 (2005).
- <sup>21</sup> V. K. Kalevich, A. Y. Shiryaev, E. L. Ivchenko, A. Y. Egorov, L. Lombez, D. Lagarde, X. Marie, and T. Amand, JETP Letters **85**, 174 (2007).
- <sup>22</sup> X. J. Wang, Y. Puttisong, C. W. Tu, A. J. Ptak, V. K. Kalevich, A. Y. Egorov, L. Geelhaar, H. Riechert, W. M. Chen, and I. A. Buyanova, Appl. Phys. Lett. **95**, 241904 (2009), <http://dx.doi.org/10.1063/1.3275703>.
- <sup>23</sup> H. M. Zhao, L. Lombez, B. L. Liu, B. Q. Sun, Q. K. Xue, D. M. Chen, and X. Marie, Appl. Phys. Lett. **95**, 041911 (2009), <http://dx.doi.org/10.1063/1.3186076>.
- <sup>24</sup> F. Zhao, A. Balocchi, A. Kunold, J. Carrey, H. Carre, T. Amand, N. Ben Abdallah, J. C. Harmand, and X. Marie, Appl. Phys. Lett. **95**, 241104 (2009), <http://dx.doi.org/10.1063/1.3273393>.
- <sup>25</sup> F. Zhao, A. Balocchi, G. Truong, T. Amand, X. Marie, X. J. Wang, I. A. Buyanova, W. M. Chen, and J. C. Harmand, J. Phys.: Condens. Matter **21**, 174211 (2009).
- <sup>26</sup> Y. Puttisong, X. J. Wang, I. A. Buyanova, H. Carre, F. Zhao, A. Balocchi, X. Marie, C. W. Tu, and W. M. Chen, Appl. Phys. Lett. **96**, 052104 (2010), <http://dx.doi.org/10.1063/1.3299015>.
- <sup>27</sup> E. L. Ivchenko, V. K. Kalevich, A. Y. Shiryaev, M. M. Afanasiev, and Y. Masumoto, J. Phys.: Condens. Matter **22**, 465804 (2010).
- <sup>28</sup> D. Paget, Phys. Rev. B **30**, 931 (1984).
- <sup>29</sup> C. Weisbuch and G. Lampel, Solid State Commun. **14**, 141 (1974).
- <sup>30</sup> C. T. Nguyen, A. Balocchi, D. Lagarde, T. T. Zhang, H. Carre, S. Mazzucato, P. Barate, E. Galopin, J. Gierak, E. Bourhis, J. C. Harmand, T. Amand, and X. Marie, Appl. Phys. Lett. **103**, 052403 (2013), <http://dx.doi.org/10.1063/1.4816970>.
- <sup>31</sup> A. Kunold, A. Balocchi, F. Zhao, T. Amand, N. B. Abdallah, J. C. Harmand, and X. Marie, Phys. Rev. B **83**, 165202 (2011).
- <sup>32</sup> V. K. Kalevich, M. M. Afanasiev, A. Y. Shiryaev, and A. Y. Egorov, Phys. Rev. B **85**, 035205 (2012).
- <sup>33</sup> V. K. Kalevich, M. M. Afanasiev, A. Y. Shiryaev, and A. Y. Egorov, JETP Letters **96**, 567 (2012).
- <sup>34</sup> Y. Puttisong, X. J. Wang, I. A. Buyanova, and W. M. Chen, Phys. Rev. B **87**, 125202 (2013).
- <sup>35</sup> Y. Puttisong, X. J. Wang, I. A. Buyanova, L. Geelhaar, H. Riechert, A. J. Ptak, C. W. Tu, and W. M. Chen, Nat. Commun. **4**, 1751 (2013).
- <sup>36</sup> C. Sandoval-Santana, A. Balocchi, T. Amand, J. C. Harmand, A. Kunold, and X. Marie, Phys. Rev. B **90**, 115205 (2014).
- <sup>37</sup> E. L. Ivchenko, L. A. Bakaleinikov, and V. K. Kalevich, Phys. Rev. B **91**, 205202 (2015).
- <sup>38</sup> R. K. Wangsness and F. Bloch, Phys. Rev. **89**, 728 (1953).
- <sup>39</sup> A. Redfield, in *Advances in Magnetic Resonance*, Advances in Magnetic and Optical Resonance, Vol. 1, edited by J. S. Waugh (Academic Press, 1965) pp. 1 – 32.
- <sup>40</sup> G. W. Leppelmeier and E. L. Hahn, Phys. Rev. **142**, 179 (1966).
- <sup>41</sup> J. Kowalewski and L. Maler, *Nuclear Spin Relaxation in Liquids: Theory, Experiments, and Applications*, Series in Chemical Physics (CRC Press, 2006) Chap. 4.
- <sup>42</sup> N. A. Sinitsyn, Y. Li, S. A. Crooker, A. Saxena, and D. L. Smith, Phys. Rev. Lett. **109**, 166605 (2012).
- <sup>43</sup> D. J. Hilton and C. L. Tang, Phys. Rev. Lett. **89**, 146601 (2002).
- <sup>44</sup> V. Kalevich, A. Y. Shiryaev, E. Ivchenko, M. Afanasiev, A. Y. Egorov, V. Ustinov, and Y. Masumoto, Physica B **404**, 4929 (2009).
- <sup>45</sup> D. Lagarde, L. Lombez, X. Marie, A. Balocchi, T. Amand,

V. K. Kalevich, A. Shiryayev, E. Ivchenko, and A. Egorov,  
Phys. Status Solidi A **204**, 208 (2007).